Quantum Brownian Motion at Strong Dissipation Probed by Superconducting Tunnel Junctions

Berthold Jäck,[1,*] Jacob Senkpiel,[1] Markus Etzkorn,[1] Joachim Ankerhold,[2] Christian R. Ast,[1] and Klaus Kern[1,3]
[1]Max-Planck-Institut für Festkörperforschung, 70569 Stuttgart, Germany
[2]Institut für Komplexe Quantensysteme and IQST, Universität Ulm, 89069 Ulm, Germany
[3]Institut de Physique de la Matière Condensée, Ecole Polytechnique Fédérale de Lausanne, 1015 Lausanne, Switzerland
(Received 15 January 2017; revised manuscript received 15 May 2017; published 4 October 2017)

We have investigated the phase dynamics of a superconducting tunnel junction at ultralow temperatures in the presence of high damping, where the interaction with environmental degrees of freedom represents the leading energy scale. In this regime, theory predicts the dynamics to follow a generalization of the classical Smoluchowski description, the quantum Smoluchowski equation, thus, exhibiting overdamped quantum Brownian motion characteristics. For this purpose, we have performed current-biased measurements on the small-capacitance Josephson junction of a scanning tunneling microscope placed in a low impedance environment at milli-Kelvin temperatures. We can describe our experimental findings with high accuracy by using a quantum phase diffusion model based on the quantum Smoluchowski equation. In this way we experimentally demonstrate that overdamped quantum systems follow quasiclassical dynamics with significant quantum effects as the leading corrections.

DOI: 10.1103/PhysRevLett.119.147702

Introduction.—Brownian motion—that is, the fate of a heavy particle immersed in a fluid of lighter particles—is the prototype of a dissipative system coupled to a thermal bath [1]. Its quantum mechanical analogue can be found in open quantum systems, which have received considerable attention in the last decade [2]. This is mainly due to the experimental progress in fabricating quantum devices on ever-growing scales with the intention to control their quantum properties to an unprecedented accuracy. Efforts have thus focused to tame the impact of decoherence and noise in order to preserve fragile features such as entanglement as possible resources for technological applications [3].

The regime where dissipation cannot be seen as a perturbation but tends to completely dominate the system dynamics has received much less attention. This is in sharp contrast to classical nonequilibrium dynamics, where the so-called overdamped regime, also known as the classical Smoluchowski regime (CSM), plays a pivotal role for diffusion phenomena in a broad variety of realizations [1]. Theoretically, this domain is characterized by a separation of time scales between the relaxation of momentum (fast) and the relaxation of position (much slower), implying that on a coarsely grained time scale the latter constitutes the only relevant degree of freedom. The situation in quantum mechanics is more subtle though. Position and momentum are bound together by Heisenberg's uncertainty relation, which is detrimental to the tendency of strong dissipation to induce localization and even dissipative phase transitions [4,5].

Roughly speaking, a dissipative quantum system is characterized by three typical energy scales, namely, an excitation energy $\hbar\omega_0$, where ω_0 denotes some specific energy scale of the bare system and $\hbar$ the reduced Planck's constant, a coupling energy to the environment $\hbar\gamma$, where γ denotes the coupling parameter, and the thermal energy k_BT with k_B as Boltzmann's constant and T as the temperature. While the realm of classical physics is defined by $\hbar\gamma, \hbar\omega_0 \ll k_BT$, the predominantly explored quantum domain of weak system-bath interaction obeys $\hbar\gamma \ll k_BT \ll \hbar\omega_0$ with the bare level spacing exceeding all other energy scales. This is the generic situation for cavity and circuit quantum electrodynamical setups [2].

The quantum range of strong dissipation is complementary, i.e., $k_BT \ll \hbar\omega_0 \ll \hbar\gamma$. It has been predicted by theory that in this domain a separation of time scales and thus a quantum Smoluchowski regime (QSM) exists indeed [6]. Quantum Brownian motion in the QSM is almost classical; however, it is substantially influenced by quantum fluctuations yielding overdamped quantum phase diffusion (OQPD) characteristics. Consequently, in all processes sensitive to these fluctuations the dynamics is predicted to deviate strongly from the classical one. Hence, exploring the QSM regime is not only of fundamental interest, but is also of direct relevance for systems possibly subject to strong dissipation, such as low impedance superconducting circuits [7], nanomechanical oscillators [8], quantum gases [9], quantum annealing computers [10], or chemical reactions in solution. Yet, its experimental observation has been elusive so far.

The aim of this Letter is to close this gap. For this purpose, we study the dynamics of the phase ϕ as a continuous collective degree of freedom in a superconducting tunnel junction in the QSM regime. In the past, superconducting circuits have proven to serve as ideal test beds to explore quantum dissipative phenomena such as

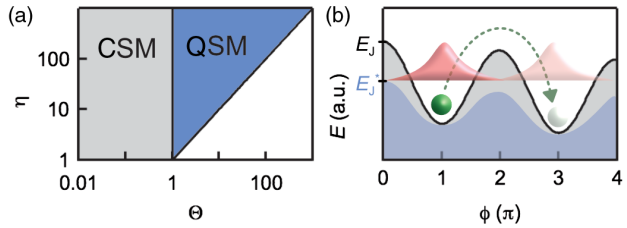

FIG. 1. (a) Parameter diagram for the dynamics of overdamped diffusion $\eta = \gamma^2/\omega_0^2 > 1$: The regime of OQPD (QSM) emerges at lower temperatures from the CSM when the dimensionless friction η sufficiently exceeds the dimensionless inverse temperature $\Theta = \gamma\hbar\beta/(2\pi) \gg 1$. (b) The phase dynamics corresponds to the dissipative quantum dynamics of a particle in a washboard potential (grey solid), which appears as MQT for weak friction, i.e., the tunneling of the phase wave function through the potential wall (red wave package), and as OQPD in the QSM domain, for which quantum fluctuations effectively reduce the barrier height (blue solid). Classical phase diffusion at $\Theta \ll 1$ is illustrated as the thermally activated escape of a particle (green dot) over the potential barrier.

macroscopic quantum tunneling (MQT) and underdamped quantum phase diffusion (UQPD) [11–15], as well as dephasing and decoherence phenomena [16,17]. Here, we access the hitherto untouched QSM domain by investigating the current-voltage characteristics (IVC) of current-biased small capacitance tunnel junctions in an ultralow temperature scanning tunneling microscope (STM) [18]. Its phase dynamics is equivalent to quantum diffusion along a tilted washboard potential under strong damping, cf. Fig. 1(b), referring to a low impedance environment with Ohmic resistance $R_{\rm dc}$ much smaller than the quantum resistance $R_Q = h/4e^2$, i.e., $\rho \equiv R_{\rm dc}/R_Q \ll 1$ (e denotes the elementary charge) [19,20]. Accessing the QSM regime shown in Fig. 1(a) where OQPD can be observed requires that the dimensionless friction $\eta = \gamma^2/\omega_0^2$ sufficiently exceeds the dimensionless inverse temperature $\Theta = \gamma\hbar\beta/(2\pi) \gg 1$ [21]. Expressed in junction parameters this corresponds to

$$\eta \equiv \frac{E_C}{2\pi^2\rho^2 E_J} \gg \Theta \equiv \frac{\beta E_C}{2\pi^2\rho} \gg 1, \tag{1}$$

with charging energy E_C, tunnel coupling E_J, and inverse temperature $\beta = 1/k_B T$ [20]. For a Cooper pair transfer, the charging energy reads as $E_C = (2e)^2/2C_J = 2e^2/C_J$, where C_J denotes the junction capacitance. The mechanical damping parameter γ relates to the junction parameters as $\gamma = \sqrt{\eta}\omega_0 = E_C/\hbar\pi\rho$, with ω_0 as the Josephson plasma frequency $\omega_0 = \sqrt{2eI_0/\hbar C_J}$ and the critical current $I_0 = 2eE_J/\hbar$ [20]. The condition in Eq. (1) is essentially always fulfilled for small capacitance tunnel junctions operated at milli-Kelvin temperatures in a low impedance environment $\rho \ll 1$ [22]. We note that previous STM studies successfully observed classical overdamped phase diffusion in the CSM regime at $\Theta \ll 1$ [23,24], whose dynamics are characterized by the McCumber parameter $\beta_C = 1/\eta$ [25].

Theory.—The supercurrent through a superconducting tunnel junction is determined by its phase dynamics according to the first Josephson relation, $I_J = I_0 \sin(\phi)$. In the QSM regime the diffusion of the phase ϕ occurs in a washboard potential tilted by a bias current I_B as depicted in Fig. 1(b) [19,20]. Below the switching current I_S, the phase diffuses from one well to another due to the interplay of thermal and quantum fluctuations, this way acquiring a finite velocity $\dot{\phi} \neq 0$, cf. Fig. 1(b). According to Josephson's second relation, $\langle\dot{\phi}\rangle = (2e/\hbar)V$, this velocity relates to a measurable voltage drop across the junction. The corresponding Cooper pair current takes the compact form

$$I_J^{\rm QSM} = \frac{e\rho\beta\pi}{\hbar}(E_J^*)^2 \frac{\beta eV}{(\beta eV)^2 + \pi^2\rho^2}, \tag{2}$$

with a renormalized tunnel coupling

$$E_J^* = E_J \rho^\rho \left(\frac{\beta E_C}{2\pi^2}\right)^{-\rho} e^{-\rho c_0}, \tag{3}$$

where $c_0 = 0.5772\ldots$ denotes Euler's constant [19,20]. The above expression can be understood as the quantum generalization of the corresponding classical Smoluchowski type of treatment for thermal phase diffusion, the Ivanchenko-Z'ilberman approach [26], by replacing E_J with its renormalized value E_J^*. The explicit dependence of E_J^* on E_C in Eq. (3) reflects the impact of charge fluctuations on the phase dynamics and thus, in the mechanical analogue, the presence of momentum fluctuations in the overdamped diffusion of position. The simultaneous interplay of classical and quantum diffusion leading to Eq. (2), therefore, corresponds to quantum Brownian motion dynamics. The physical interpretation is that quantum phase fluctuations close to the top of the washboard potential barrier depicted in Fig. 1(b) effectively reduce its height considerably [20]. One may see this effect as complementary to MQT occurring at low temperatures and weak damping in the opposite domain, $E_J > E_C$ [13–15].

As demonstrated theoretically, in the QSM regime quantum phase fluctuations substantially reduce I_S much below I_0 [19,20]. We employ this effect as an experimental probe for the detection of OQPD and to distinguish it from its classical counterpart.

Superconducting circuit.—The circuit diagram of our experiment is depicted in Fig. 2(a). The atomic-scale tunnel junction appears between a superconducting vanadium STM tip and a superconducting vanadium (100) single crystal surface, having a capacitance C_J on the order of one femtofarad [22]. The junction and its direct electromagnetic environment, $Z(\nu)$, are thermalized at the base temperature of the dilution refrigerator STM, $T = 15$ mK [18]. A typical IVC measured at a normal state conductivity $G_N = 0.004G_0$ with $G_0 = 1/(2R_Q)$ is shown

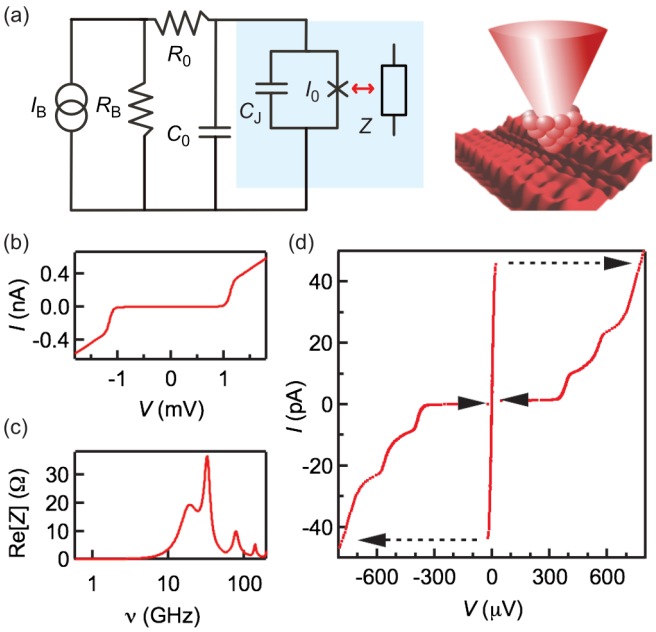

FIG. 2. (a) Circuit diagram with the current source I_B, the source impedance R_B, the load-line resistor and shunt capacitor R_0 and C_0, respectively. The junction and its direct environment thermalized at $T = 15$ mK are highlighted by the blue box. I_0 and C_J denote the junction element and capacitor, respectively, and Z the environmental impedance. Right: Schematic representation of the STM tip on top of the reconstructed $V(100)$ surface [22]. (b) IVC measured at $G_N = 0.004G_0$. (c) Simulated real part $\Re[Z(\nu)]$ of the environmental impedance [28]. (d) In-gap region of an IVC from a current-biased measurement at $G_N = 0.074G_0$.

in Fig. 2(b) and exhibits a well-developed superconducting gap [27]. Details of the sample preparation and measurement procedure can be found in Refs. [22,31], respectively.

We separate the time scales of biasing circuit $\tau_{RC} \approx R_0C_0$ and junction phase, $\tau_\phi = 2\pi/\omega_0 \approx 10^{-11}$ s, by using a large shunt capacitor $C_0 = 3$ nF and load-line resistor of $R_0 = 3.5$ kΩ and obtain $\tau_{RC} \approx 10^{-5} \gg \tau_\phi$ [28,36]. Concerning $Z(\nu)$, its dc part is dominated by the coupling of the tunneling Cooper pairs to the electromagnetic vacuum in the gap between tip and sample (tunnel barrier), the STM being operated in ultrahigh vacuum. Thus, the vacuum impedance $R_{dc} = Z(\nu \to 0) = 377\ \Omega$ determines the dc impedance in the vicinity of the tunnel junction whereas the resistance of the leads (transmission lines) is negligibly small [22]. In this way we realize $\rho \ll 1$ and as such the strong damping at ω_0. Additionally, we obtain an effective dc impedance for low GHz frequencies by choosing an STM tip of adequate length. This moves the tip resonance modes in $Z(\nu)$ to $\nu > 10$ GHz, as is illustrated in Fig. 2(c) [28] and we can apply Eq. (2) to describe IVC small voltages around 0 in our experiment [37].

Results.—Figure 2(d) displays an IVC measured at $G_N = 0.074G_0$ to illustrate the general properties of our setup. For increasing bias current starting from 0, the IVC follows a phase diffusion branch at $V \neq 0$, before switching to a dissipative in-gap current at $I = I_S$. Owing to the large source resistance, $R_B = 1.33$ GΩ, the circuit features an almost horizontal load line [38]. For decreasing bias currents starting from $I > I_S$, the IVC follows the in-gap current, which originates from lifetime effects of Cooper pairs in the STM tip and incoherent Cooper pair tunneling [28–30], before returning into the phase diffusion branch at I_R. The occurrence of a hysteretic IVC with $I_S \gg I_R$ reflects the strong frequency dependent damping of our circuit, which is similar to Refs. [39,40] yet exhibits strong damping at ω_0 due to $\rho \ll 1$.

To determine the physical processes leading to the phase diffusion branch in Fig. 2(d), we record a series of IVCs measured at 13 different G_N/G_0 values, $0.05 < G_N/G_0 < 0.3$. Varying G_N/G_0 at fixed temperature provides us an ideal handle to tune $\eta \propto E_J^{-1} \propto G_N^{-1}$ along a vertical axis in the phase diagram in Fig. 1(a). In Fig. 3(a), we present IVCs measured at different G_N/G_0 values and focus on small voltages $V < 30\ \mu$V for $I > 0$. Towards higher G_N/G_0 values, we observe a nonlinear increase of I_S. This is illustrated in Fig. 3(b), where we plot the extracted I_S values as a function of G_N/G_0 and fit a quadratic dependence $I_S \propto G_N^2$, as predicted by Eq. (2). Additionally, we find I_S strongly reduced in comparison to calculated critical current $I_0 \propto G_N$ values for all measurements in Fig. 3(b) [22,31,41]. With thermal energy being comparatively small $E_J\beta \geq 5$ [22,31], classical thermally activated phase diffusion cannot be the dominant process. Instead, this strong reduction of I_S and the $I_S \propto G_N^2$ scaling indicate the major relevance of quantum effects for the diffusion dynamics.

Similar behavior has been reported for underdamped junctions in the regime $E_C \geq E_J$, where diffusion was found to be dominated by MQT of the phase, corresponding to UQPD [42,43]. To quantify the relevance of MQT for the diffusion dynamics in our experiment, we compare the experimental zero bias resistance, $R_{ZB,exp}$ with calculated values, $R_{ZB,MQT}$, as they would result from UQPD [31,42,43]. As can be seen in Fig. 3(c), $R_{ZB,exp}$ is qualitatively and quantitatively different from $R_{ZB,MQT}$. While $R_{ZB,MQT}$ tends to flatten out towards larger E_C/E_J values, $R_{ZB,exp}$ fits very well to an $(E_C/E_J)^2$ scaling as predicted for OQPD [19,20]. Hence, all our experimental findings support the major relevance of quantum fluctuations for the diffusion dynamics as they appear in the OQPD regime.

To quantitatively analyze the experimental IVCs using the OQPD model in Eq. (2), we determine the experimental parameters by performing additional voltage-biased measurements. Fitting these IVCs with $P(E)$ theory [44,45], we determine the T, E_J, E_C, and R_{dc} values with high precision, which are summarized in Table I; for details see Ref. [31]. Owing to the small junction capacitance C_J, thermally induced capacitive noise broadens the measured IVCs. We account for this effect by convolving the calculated IVC from Eq. (2) with a normalized Gaussian

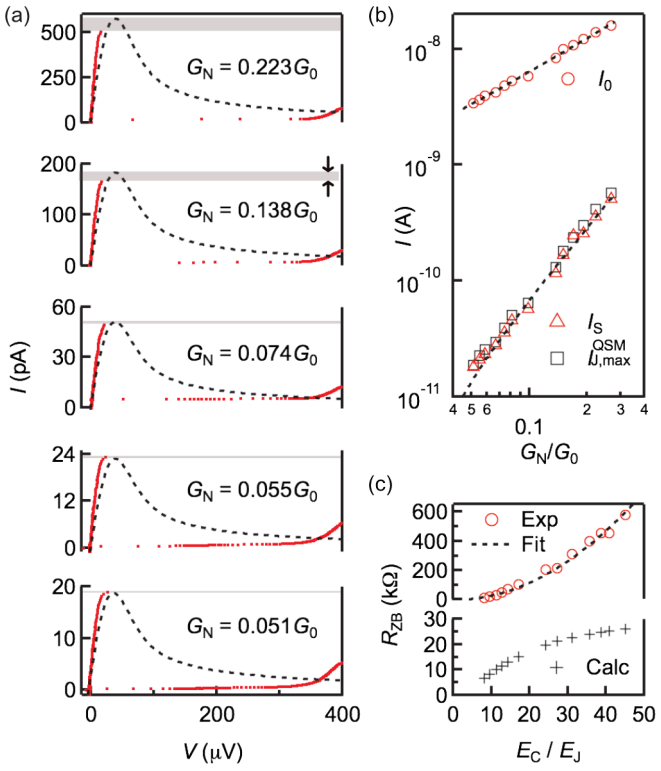

FIG. 3. (a) Experimental (red dots) and calculated (dashed lines) IVCs at indicated values of G_N/G_0. The deviation between I_S and $I^{QSM}_{J,max}$ is highlighted via the grey bars. (b) Top: Calculated I_0 (open circles) and linear fit (dashed line) as a function of G_N/G_0. Bottom: Experimental, I_S (open triangles), and calculated switching current, $I^{QSM}_{J,max}$ (open squares), as well as a quadratic fit (dashed line) as a function of G_N/G_0. Error bars are contained within the symbols. (c) Experimental (Exp, open circles) and calculated from MQT (Calc, plus signs) zero bias resistance as well as a square fit to the experimental data (Fit, dashed line) as a function of E_C/E_J.

of width $\sigma = \sqrt{2E_C/\beta}$ [22,46]. This enables us to calculate IVCs by using the OQPD model in Eq. (2) without free parameters for each G_N/G_0 value.

In Fig. 3(a), we compare experimental and calculated IVCs at $V < 30\ \mu$V. While we find excellent quantitative agreement regarding I_S for small G_N/G_0 values, we find the zero bias resistance of the calculated curve, $R_{ZB,QSM}$ to be slightly larger than the experimental value, $R_{ZB,exp}$. By contrast, considering the IVCs measured at high G_N values, we observe significant quantitative deviations in the current amplitude between theory and experiment. We analyze those deviations in the following in more detail and compare our experimental data with a classical diffusion model.

Discussion.—We start our discussion by comparing I_S with the maximum of the calculated IVC, $I^{QSM}_{J,max}$, as a measure for the agreement between experiment and theory. In Fig. 4(a), we plot their relative deviation $\Delta I_{QSM} = |I^{QSM}_{J,max} - I_S|/I^{QSM}_{J,max}$ as a function of G_N/G_0. Furthermore, we calculate the conditions for the QSM regime, Eq. (1), by using the same set of parameters from the $P(E)$ fits as before. We obtain $\Theta = 122$ and plot the dependence of η/Θ on G_N/G_0 in Fig. 4(a). At low conductivities, the condition for QSM dynamics is fulfilled $\eta/\Theta > 5$, explaining the very good agreement between theory and experiment, $3\% < \Delta I_{QSM} < 9\%$. By contrast, we find $\Delta I_{QSM} > 12\%$ at high conductivities. In this regime, the condition for a separation of time scales of position and momentum dynamics is violated $\eta/\Theta \approx 1$, and the QSM equation is not applicable. Regarding the slope of the phase diffusion branch, we attribute the small deviations between $R_{ZB,exp}$ and $R_{ZB,QSM}$ to small deviations of $Z(\nu)$ from perfect dc behavior required for the derivation of Eq. (2), cf. Fig. 2(c). It appears less likely that theory overestimates the influence of quantum fluctuations. While this would explain $R_{ZB,QSM} > R_{ZB,exp}$, it reduces $I^{QSM}_{J,max}$ at the same time, which contradicts our data.

Additionally, we compare our experimental data with the classical Ivanchenko-Zil'berman model (CIZ), in which phase diffusion only occurs via thermally activated escape over the washboard potential barrier, displaying classical Brownian motion dynamics, cf. Fig. 1(b) [26,47]. We present an experimental IVC together with a calculated IVC using the CIZ model and the same parameter set from $P(E)$ theory as before in Fig. 4(b). As can be seen, theory based on classical diffusion largely overestimates the experimental switching current. This observation underlines the high relevance of quantum fluctuations,

TABLE I. Mixing chamber temperature T_{MC}, environmental dc impedance R_{dc}, as well as the fitted temperature T, charging energy E_C, and tunnel coupling E_J obtained from $P(E)$ fits, cf., Ref. [31].

Experiment		$P(E)$ fits		
T_{MC} (mK)	R_{dc} (Ω)	T (mK)	E_C (μeV)	E_J (μeV)
15	377	20.8 ± 0.2	252 ± 3	$5.6 \pm 0.3 \ldots 31 \pm 1.6$

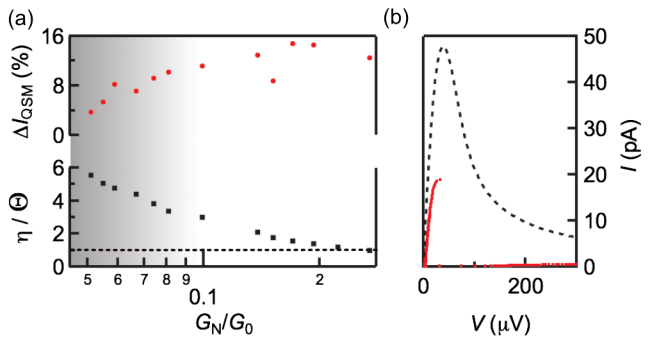

FIG. 4. (a) Relative deviation between theoretical and experimental current maxima ΔI_{QSM} and ratio η/Θ as a function of G_N/G_0. The QSM regime boundary is marked as a dashed line at $\eta/\Theta = 1$. (b) Comparison between experimental (dots) and calculated IVC (dashed line) from the purely classical CIZ model at $G_N = 0.051G_0$.

significantly reducing the washboard potential barrier height and thus I_S in comparison to purely classical thermal phase diffusion.

Conclusion.—We studied the dynamics of a quantum system for which the system-bath interaction represents the leading energy scale (QSM regime). For this purpose, we investigated the phase dynamics of a small-capacitance Josephson junction in a STM placed in a low impedance environment at ultralow temperatures by means of current-biased experiments. Experimental current-voltage characteristics can be described by using a OQPD model with high accuracy in agreement with theoretical predictions. This in turn reveals that quantum systems in the QSM regime exhibit quasiclassical dynamics with significant quantum-mechanical corrections in leading order that is quantum Brownian motion [6]. Our analysis complements extensive studies on underdamped systems, where phenomena such as quantum tunneling occur [14,15]. While these processes are suppressed at strong dissipation, the impact of quantum fluctuations induced by the system-reservoir coupling is substantial in this regime. In addition, our study demonstrates the unique potential of ultralow temperature STM to address questions in the field of mesoscopic transport and quantum statistics. We envision that future experiments should reveal the temperature-dependent transition from QSM to CSM dynamics.

It is our pleasure to acknowledge inspiring discussions with P. W. Anderson, D. Esteve, J. Pekola, F. Tafuri, M. Ternes, S. Kochen, and A. Yazdani. Financial support was provided by the Center for Integrated Quantum Science and Technology (IQ^{ST}) (J. A., C. A., K. K.) and the German Science Foundation (DFG) through Grant No. AN336/11-1 (J. A.)

*Corresponding author.
berthold.jack@alumni.epfl.ch
Present address: Princeton University, Joseph Henry Laboratory at the Department of Physics, Princeton, NJ 08544, USA.

[1] H. Risken, *The Fokker Planck Equation*, Springer Series in Synergetics Vol. 18 (Springer, Berlin, 1984).
[2] R. J. Schoelkopf and S. M. Girvin, Nature (London) **451**, 664 (2008).
[3] M. H. Devoret and R. J. Schoelkopf, Science **339**, 1169 (2013).
[4] A. Schmid, Phys. Rev. Lett. **51**, 1506 (1983).
[5] U. Weiss, *Quantum Dissipative Systems* (World Scientific, Singapore, 1999).
[6] J. Ankerhold, P. Pechukas, and H. Grabert, Phys. Rev. Lett. **87**, 086802 (2001); **99**, 139901 (2007).
[7] M. F. Goffman, R. Cron, A. Levy Yeyati, P. Joyez, M. H. Devoret, D. Esteve, and C. Urbina, Phys. Rev. Lett. **85**, 170 (2000).
[8] M. Aspelmeyer, T. J. Kippenberg, and F. Marquardt, Rev. Mod. Phys. **86**, 1391 (2014).
[9] I. Bloch, J. Dalibard, and W. Zwerger, Rev. Mod. Phys. **80**, 885 (2008).
[10] N. G. Dickson, M. W. Johnson, M. H. Amin, R. Harris, F. Altomare, A. J. Berkley, P. Bunyk, J. Cai, E. M. Chapple, P. Chavez *et al.*, Nat. Commun. **4**, 1903 (2013).
[11] M. Simmonds and W. H. Parker, Phys. Rev. Lett. **24**, 876 (1970).
[12] A. O. Caldeira and A. J. Leggett, Phys. Rev. Lett. **46**, 211 (1981).
[13] M. H. Devoret, J. M. Martinis, and J. Clarke, Phys. Rev. Lett. **55**, 1908 (1985).
[14] J. M. Kivioja, T. E. Nieminen, J. Claudon, O. Buisson, F. W. J. Hekking, and J. P. Pekola, Phys. Rev. Lett. **94**, 247002 (2005).
[15] H. F. Yu, X. B. Zhu, Z. H. Peng, Y. Tian, D. J. Cui, G. H. Chen, D. N. Zheng, X. N. Jing, L. Lu, S. P. Zhao, and S. Han, Phys. Rev. Lett. **107**, 067004 (2011).
[16] P. Bertet, I. Chiorescu, G. Burkard, K. Semba, C. J. P. M. Harmans, D. P. DiVincenzo, and J. E. Mooij, Phys. Rev. Lett. **95**, 257002 (2005).
[17] G. Ithier, E. Collin, P. Joyez, P. J. Meeson, D. Vion, D. Esteve, F. Chiarello, A. Shnirman, Y. Makhlin, J. Schriefl, and G. Schön, Phys. Rev. B **72**, 134519 (2005).
[18] M. Assig, M. Etzkorn, A. Enders, W. Stiepany, C. R. Ast, and K. Kern, Rev. Sci. Instrum. **84**, 033903 (2013).
[19] H. Grabert, G.-L. Ingold, and B. Paul, Europhys. Lett. **44**, 360 (1998).
[20] J. Ankerhold, Europhys. Lett. **67**, 280 (2004).
[21] J. Ankerhold, *Quantum Tunneling in Complex Systems*, Springer Tracts in Modern Physics Vol. 224 (Springer, Berlin Heidelberg, 2007).
[22] B. Jäck, M. Eltschka, M. Assig, M. Etzkorn, C. R. Ast, and K. Kern, Phys. Rev. B **93**, 020504 (2016).
[23] O. Naaman, W. Teizer, and R. C. Dynes, Phys. Rev. Lett. **87**, 097004 (2001).
[24] Th. Proslier, A. Kohen, Y. Noat, T. Cren, D. Roditchev, and W. Sacks, Europhys. Lett. **73**, 962 (2006).
[25] D. E. McCumber, J. Appl. Phys. **39**, 3113 (1968).
[26] Y. M. Ivanchenko and L. A. Zil'berman, Sov. Phys. JETP **28**, 1272 (1969).
[27] The STM tip gap $\Delta_1 = 341 \pm 11\,\mu$eV is reduced by approximately 57% compared to the sample gap $\Delta_2 = 800 \pm 11\,\mu$eV. This reduction is a common occurrence in STM tips; for details see [28–30].
[28] B. Jäck, M. Eltschka, M. Assig, A. Hardock, M. Etzkorn, C. R. Ast, and K. Kern, Appl. Phys. Lett. **106**, 013109 (2015).
[29] M. Eltschka, B. Jäck, M. Assig, O. V. Kondrashov, M. A. Skvortsov, M. Etzkorn, C. R. Ast, and K. Kern, Nano Lett. **14**, 7171 (2014).
[30] M. Eltschka, B. Jäck, M. Assig, O. V. Kondrashov, M. A. Skvortsov, M. Etzkorn, C. R. Ast, and K. Kern, Appl. Phys. Lett. **107**, 122601 (2015).
[31] See Supplemental Material http://link.aps.org/supplemental/10.1103/PhysRevLett.119.147702 for details on the measurement procedure, additional measurements and the $P(E)$ analysis, the calculation of R_{ZB}, and notes on the electron temperature. The Supplemental Material also includes Refs. [32–35].
[32] A. Steinbach, P. Joyez, A. Cottet, D. Esteve, M. H. Devoret, M. E. Huber, and J. M. Martinis, Phys. Rev. Lett. **87**, 137003 (2001).
[33] T. Holst, D. Esteve, C. Urbina, and M. H. Devoret, Phys. Rev. Lett. **73**, 3455 (1994).

[34] G.-L. Ingold and H. Grabert, Europhys. Lett. **14**, 371 (1991).
[35] G.-L. Ingold and Yu V. Nazarov, in *Single Charge Tunneling*, NATO ASI Series B Vol. 294 (Plenum Press, New York, 1992), Chap. 2, p. 22.
[36] P. Joyez, D. Vion, M. Götz, M. Devoret, and D. Esteve, J. Supercond. **12**, 757 (1999).
[37] G. L. Ingold, H. Grabert, and U. Eberhardt, Phys. Rev. B **50**, 395 (1994).
[38] Deviations from perfect horizontal behavior is observed for the retrapping events of the IVCs at low G_N/G_0 values. Here, incoherent Cooper pair transfer influences the retrapping process, an effect that is less pronounced for high G_N/G_0 values.
[39] J. M. Martinis and R. L. Kautz, Phys. Rev. Lett. **63**, 1507 (1989).
[40] R. L. Kautz and J. M. Martinis, Phys. Rev. B **42**, 9903 (1990).
[41] V. Ambegaokar and A. Baratoff, Phys. Rev. Lett. **10**, 486 (1963).
[42] M. Iansiti, A. T. Johnson, W. F. Smith, H. Rogalla, C. J. Lobb, and M. Tinkham, Phys. Rev. Lett. **59**, 489 (1987).
[43] M. Iansiti, M. Tinkham, A. T. Johnson, W. F. Smith, and C. J. Lobb, Phys. Rev. B **39**, 6465 (1989).
[44] M. H. Devoret, D. Esteve, H. Grabert, G.-L. Ingold, H. Pothier, and C. Urbina, Phys. Rev. Lett. **64**, 1824 (1990).
[45] D. Averin, Y. Nazarov, and A. A. Odintsov, Physica (Amsterdam) **165–166B**, 945 (1990).
[46] C. R. Ast, B. Jäck, J. Senkpiel, M. Eltschka, M. Etzkorn, J. Ankerhold, and K. Kern, Nat. Commun. **7**, 13009 (2016).
[47] V. Ambegaokar and B. I. Halperin, Phys. Rev. Lett. **22**, 1364 (1969).